Journal of Crystal Growth 51 (1981) 251–266

MACROSCOPIC CZOCHRALSKI GROWTH

I. Theoretical investigation, heat flow and growth model

A. VAN DER HART and W. UELHOFF
Institut für Festkörperforschung der KFA Jülich, D-5170 Jülich, W. Germany

Received 27 December 1979; manuscript received in final form 5 May 1980

The application of a slice model allows an exact description of the geometrical shape of Czochralski grown crystals, including the shape of the seed holder, the seed, the neck, the crystal and the transition zones between the seed and the neck and between the neck and the crystal. A one-dimensional differential equation to describe the heat transfer in the Czochralski process is set up. It is solved by taking into account heat transport due to radiation and convection, with surrounding temperatures calculated by using the correct expressions of the view factors and the radiation equations without linearization. Together with the basic growth equations of meniscus-controlled growth this model enables us to calculate interesting local quantities for any growth stage, as e.g. temperature distribution, axial and radial temperature gradients, local strains and stresses. The important interfacial growth parameters as a function of the time and crystal length are also computed. Especially, the bulk melt temperature–time program for achieving a desired crystal shape can be predicted. The computed results for three metal crystals with different shapes are given and compared with those of earlier published models.

1. Introduction

In contrast to crystal growth in crucibles, the purely meniscus-controlled growth of the Czochralski and the floating zone processes is much more complicated: The crystal shape is strongly dependent upon two general factors: (1) the heat flow condition, (2) the meniscus configuration. The position of the solid–liquid interface is controlled particularly by the first factor and this position controls radial and axial growth.

In this paper a model describing the heat flow problem in Czochralski growth and the basic equations governing the axial and the radial growth will be dealt with * [1]. In a second paper an experimental equipment for performing different growth techniques, for checking the theory and for the real time measurement of important growth parameters will be described. In a third paper [2] the growth parameters for metal crystals determined from our experiments will be compared with our theoretical values.

* This model was partly presented at the ECCG 1 in Zürich, 1976.

The investigation of these problems is important for two reasons: first, it is known that the perfection of the crystal is determined in a very complex way by some growth parameters. Their influence on the perfection is partly understood qualitatively (e.g. thermal stresses and dislocation density) and partly quantitatively (concentration of a solute, constitutional supercooling and microsegregation).

Secondly, if we understand macroscopic growth we are able to work out a basic technique to control the shaping of the crystal as required.

For example: the influence of the melt temperature on the crystal shape is important. A sudden change in the melt temperature of 1°C means, for a copper crystal with a diameter of 1 cm, a decrease or an increase of the crystal diameter of about 5% [3]. Reliable temperature control is therefore necessary. Yet in order to grow a crystal with a constant diameter, the melt temperature has also to be increased or decreased continuously during the growth process, depending on the crystal diameter (see section 8). To reach a particular crystal shape, a certain time dependence of the melt temperature is required. It is advantageous to control this melt temperature program

automatically in order to reproduce the shape.

The temperature distribution in growing crystals has already been calculated by Wilcox [4] and Brice [5] for germanium crystals, by Lallemand [6] for gallium crystals and by Kobayashi and Arizumi [7]; a review paper by Kobayashi [8] will soon be published. For all these calculations, it was assumed that the crystal had an infinite length and a constant radius. For semiconductors and insulators the assumption of infinite length may hold, because the heat conductivity for these substances is very low. This means that after a certain length, the temperature distribution does not depend on the crystal length. For germanium, e.g. this length is $6\sqrt{a}$, where a is the crystal radius [5]. However, this assumption is not realistic for metals, where heat conductivity is much higher (the heat conductivity of copper is about ten times that of germanium). Therefore the temperature distribution of metal crystals is still influenced by the crystal neck even when the crystal has reached a length of 10 cm. For this reason, all the theories neglecting the crystal neck are useless for a quantitative understanding of the growth process.

Recently Buckley-Golder and Humphrey [9] published a theoretical study of heat flow problems in Czochralski growth. The authors included the crystal neck in their calculations and published the temperature distribution and axial temperature gradient for copper and silicon. A comparison of their results with our measurements will be made in our third paper. However, Buckley-Golder's study has two severe disadvantages. First, the system worked out mathematically is only divided into three parts; secondly, the local changing of the surrounding temperature is not taken into account.

The next section of this paper will deal with the Laplace differential equation for heat flow. In section 3 a one-dimensional model describing the heat flow during Czochralski growth will be derived. In section 4 the local distribution of the surrounding temperature of the growing crystal is investigated. In section 5 the heat loss due to convection in the gas phase is described. Section 6 will deal with the numerical methods used for solving our heat flow boundary problem.

If we wish to draw the desired conclusion from the obtained temperature distribution in the crystal we must discuss the temperature distribution in the bulk melt and in the liquid column of the meniscus. These problems will be looked at in section 7, together with the basic equations governing axial and radial growth and the results will then allow us to calculate some growth parameters (bulk melt temperature, temperature gradient – especially at the interface – interface curvature etc.) as a function of the time and a given crystal shape of any geometry. In this final chapter therefore we are able to predict some dependences. The validity of these dependences will be investigated in our proposed third paper.

2. The Laplace differential equation for heat flow

In the Czochralski method of growth, the material to be grown is melted in a crucible. A seed crystal is brought into contact with the melt surface and after correct wetting has been completed, it is slowly withdrawn. The crystal diameter can be increased or decreased by lowering or raising the crucible temperature respectively. Fig. 1 shows the heat flow in the system. $\dot{Q}_1$ is the heat flow from the melt to the crystal, $\dot{Q}_2$ is the heat flow into the crystal at the interface, $\dot{Q}_3$ is the latent heat of fusion developed at the interface and $\dot{Q}_4$ is the heat flow from the surface of the crystal due to radiation and additionally due to

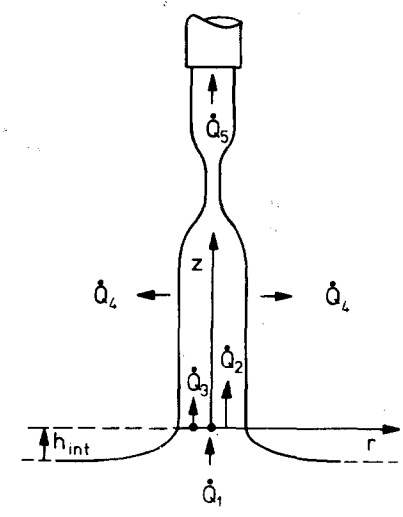

Fig. 1. The coordinate system used and the heat flow in a growing crystal: $\dot{Q}_1 + \dot{Q}_3 = \dot{Q}_2 = \dot{Q}_4 + \dot{Q}_5$.

convection, if a gas atmosphere is used and $\dot{Q}_5$ is the heat flowing into the seed holder.

By considering the rate of accumulation of heat at each point in the crystal, the general equation for the temperature may be written [10]

$$\operatorname{div}(\lambda \operatorname{grad} T(r, z, t)) = \rho c \, \mathrm{d}T(r, z, t)/\mathrm{d}t \, . \tag{1}$$

For the description of the symbols used, see the appendix. If the heat conductivity is independent of the temperature, this equation can be written for a cylindrically symmetrical system:

$$\left[\lambda\left(\frac{\partial^2}{\partial r^2} + \frac{1}{r}\frac{\partial}{\partial r} + \frac{\partial^2}{\partial z^2}\right) - v\rho c \frac{\partial}{\partial z} - \rho c \frac{\partial}{\partial t}\right] \times T(r, z, t) = 0 \, . \tag{2}$$

To decide whether the time dependent term $(\partial T(r, z, t)/\partial t)$ can be omitted, a heat diffusion length can be defined by the following equation:

$$d = \lambda / v\rho c \, .$$

If this diffusion length d is larger than the maximum crystal length, we can ignore this time dependence (i.e. $\partial T/\partial t = 0$). For metals such as copper, this length is about 500 cm, which is more than an order of magnitude larger than the length of the grown crystals. For the semiconductors silicon and germanium the time dependence can also be ignored [5]. Therefore it is justified in all these cases to use the time independent equation:

$$\left(\frac{\partial^2}{\partial r^2} + \frac{1}{r}\frac{\partial}{\partial r} + \frac{\partial^2}{\partial z^2} - \frac{v\rho c}{\lambda}\frac{\partial}{\partial z}\right) T(r, z) = 0 \, . \tag{3}$$

If the growth interface, which is at the temperature T_M, is a plane at $z = 0$ (see fig. 1), and the pulling rod with the seed holder is water cooled, the boundary conditions are

at the interface:

$$T(r, 0) = T_M \, , \quad \text{for } 0 \leqslant r \leqslant R_c \, ; \tag{4a}$$

at the crystal surface:

$$-\lambda \frac{\partial T(r, z)}{\partial r} = \dot{q}_{rad} \, , \quad \text{for } 0 \leqslant z \leqslant z_c, \; r = R_c ; \tag{4b}$$

at the seed holder:

$$T(r, z) = T_p \, , \quad \text{for } z = z_c + l_{sh}, \; 0 \leqslant r \leqslant R_{sh} ; \tag{4c}$$

at the crystal axis:

$$\partial T(r, z)/\partial r = 0 \, , \quad \text{for } r = 0. \tag{4d}$$

The heat flow in eq. (4b) is according to the Stefan–Boltzmann radiation law:

$$\dot{q}_{rad} = \epsilon\sigma[T(r, z)^4 - T_0(z)^4] \, , \quad \text{for } r = R_c .$$

To solve the differential equation (3) with the boundary conditions (4a)–(4d), it is necessary to linearize the equation of the radiation cooling:

$$\dot{q}_{rad} = h[T(R_c, z) - T_0(z)] \, . \tag{5}$$

In this equation, the factor h is still a function of the crystal temperature $T(R_c, z)$ and the so-called surrounding temperature $T_0(z)$:

$$h = \epsilon\sigma[T(R_c, z)^2 + T_0(z)^2]\,[T(R_c, z) + T_0(z)] \, . \tag{6}$$

This factor can be computed by iteration (see section 6). The boundary equation (4b) then becomes:

$$-\lambda \frac{\partial T(r, z)}{\partial r} = h[T(r, z) - T_0(z)] \, , \quad r = R_c, \; 0 \leqslant z \leqslant z_c \, . \tag{4b'}$$

For an explanation of this surrounding temperature see section 3. Since we take the local changing of the surrounding temperature and the material constants into account, introduction of the dimensionless Biot and Nusselt number would be of no advantage.

3. The heat flow model for macroscopic Czochralski growth

Eq. (3) is only solvable in an analytical form if the boundary conditions are simple (e.g. radius and surrounding temperature are independent of z). If we need to use condition (4b') and a variable crystal radius, a solution can only be obtained with extremely difficult computation methods.

To eliminate this difficulty, a further assumption has to be made. The heat flowing from the crystal axis to the surrounding walls finds two resistances:
(1) the thermal resistivity of the crystal material: R_b;
(2) the thermal surface resistivity: R_{su}.

These resistances are proportional to the thermal resistivity and the surface thermal resistivity [10] of

the material (in our case copper):

$$R_b \sim \frac{1}{\lambda} \simeq 0.3 \text{ (cm s K J}^{-1}\text{)} ,$$

$$R_{su} \sim \frac{1}{hR_c} = \frac{1}{\epsilon\sigma[T(z)+T_0(z)][T(z)+T_0(z)]R_c}$$

$$\simeq \frac{600}{R_c} \text{ (cm s K J}^{-1}\text{)} .$$

Because $R_b \ll R_{su}$ the resistance R_b can be omitted with respect to R_{su}.

Therefore we will assume that the temperature field in the crystal does not depend on the radius:

$$\left(\frac{\partial^2}{\partial r^2} + \frac{1}{r}\frac{\partial}{\partial r}\right) T(z) = 0 , \tag{7}$$

which reduces the Laplace differential equation to a one-dimensional equation. This means a much easier computation technique is possible: after the heat flow is computed, we can still calculate the mean radial temperature gradient from the heat flow and the heat conductivity.

However, because eq. (3) describes the change of the heat capacity, we have to add a term to the equation to hold the heat balance of the system yet without excluding the heat loss of the crystal surface. According to ref. [10] we can consider this heat loss as heat sink. Therefore with assumption (7) we can rewrite eq. (3):

$$\lambda \frac{\partial^2 T(z)}{\partial z^2} - v\rho c \frac{\partial T(z)}{\partial z} - \frac{\dot{Q}}{V} = 0 , \tag{8}$$

where $\dot{Q}$ is the heat loss by radiation and V is the volume of the radiating object:

$$\dot{Q} = 2\pi R_c \, \Delta z \, h[T(z) - T_0(z)] , \tag{9}$$

$$V = \pi R_c^2 \, \Delta z , \tag{10}$$

where Δz is the thickness of a slice of the crystal. If we insert expressions (9) and (10) into eq. (8) we can write:

$$\lambda \frac{\partial^2 T(z)}{\partial z^2} - v\rho c \frac{\partial T(z)}{\partial z} - \frac{2h}{R_c}[T(z) - T_0(z)] = 0 , \tag{11}$$

with the boundary conditions

at the interface:

$$T(z) = T_M , \quad z = 0 ; \tag{12a}$$

at the seed holder:

$$T(z) = T_p , \quad z = z_c + l_{sh} . \tag{12b}$$

This equation could be solved analytically if the material constants, the crystal radius, and the surrounding temperature were independent of z. In this case, the solution would be:

$$T(z) = A \exp(p_1 z) + B \exp(p_2 z) + T_0 , \tag{13a}$$

with

$$p_{1,2} = \frac{v\rho c}{2\lambda} \pm \left[\left(\frac{v\rho c}{2\lambda}\right)^2 + \frac{2h}{\lambda R_c}\right]^{1/2} . \tag{13b}$$

However, in practice, the material constants are temperature dependent, and because the temperature differences in the crystal are large, this dependence has to be taken into account. The crystal radius and the surrounding temperature are also dependent on the z-coordinate. Therefore the solution (13a)–(13b) can only be applied to small regions of the crystal. The solution of the heat flow problem of the macroscopic crystal has to be solved by a correct combination of the analytical solutions in these small regions.

This leads to the following model. The growing crystal is divided into N slices with a thickness Δz (see fig. 2). Each slice has its own radius, surrounding

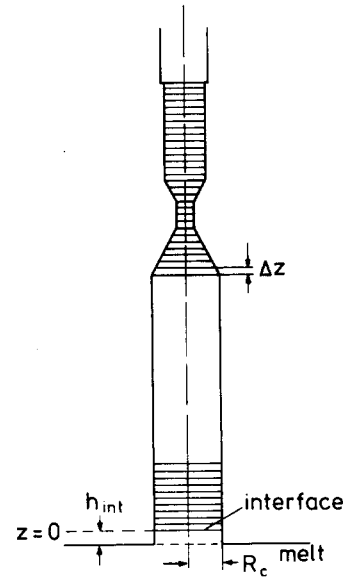

Fig. 2. The mathematical slice model.

temperature, and material constants, which can be assumed to be constant over one slice but may differ from one slice to the next. Because in each slice the above-mentioned conditions are fulfilled, the temperature distribution in slice i is given by:

$$T_i(z) = A_i \exp(p_1^{(i)} z) + B_i \exp(p_2^{(i)} z) + T_0^{(i)} , \quad (14)$$

$$p_{1,2}^{(i)} = \frac{v\rho_i c_i}{2\lambda_i} \pm \left[\left(\frac{v\rho_i c_i}{2\lambda_i}\right)^2 + \frac{2h_i}{\lambda_i R_i}\right]^{1/2} ,$$

with

$$z_{i-1} \leqslant z \leqslant z_i , \quad z_i = i\,\Delta z , \quad \text{for } i = 1, 2, ..., N. \quad (15)$$

We assume that the temperature field is continuous, so that at each boundary between two joining slices i and $i+1$, the temperature at the top of slice i equals that at the bottom of slice $i+1$:

$$T_i(z_i) = T_{i+1}(z_i) = T_i , \quad i = 1, 2, ..., N-1 . \quad (16)$$

With eq. (14) and expressions (15) and (16), the coefficients A_i and B_i can be expressed in the following way:

$$A_i = [(T_i - T_0^{(i)}) \exp(p_2^{(i)} z_{i-1}) - (T_{i-1} - T_0^{(i)}) \exp(p_2^{(i)} z_i)] \times [\exp(p_1^{(i)} z_i) \exp(p_2^{(i)} z_{i-1}) - \exp(p_1^{(i)} z_{i-1}) \exp(p_2^{(i)} z_i)]^{-1} ,$$

$$\text{for } i = 1, 2, ..., N. \quad (17a)$$

$$B_i = [(T_{i-1} - T_0^{(i)}) \exp(p_1^{(i)} z_i) - (T_i - T_0^{(i)}) \exp(p_1^{(i)} z_{i-1})] \times [\exp(p_1^{(i)} z_i) \exp(p_2^{(i)} z_{i-1}) - \exp(p_1^{(i)} z_{i-1}) \exp(p_2^{(i)} z_i)]^{-1} ,$$

$$\text{for } i = 1, 2, ..., N. \quad (17b)$$

Energy is conserved between two slices, so that the heat coming from slice i is equal to the heat passing to slice $i+1$ with an additional term for radiation $\dot{Q}_{\mathrm{rad},i,i+1}$ if the radii of the two slices are unequal (see fig. 3). The heat balance is expressed with:

$$\dot{Q}_{\mathrm{con},i} = \dot{Q}_{\mathrm{con},i+1} + \dot{Q}_{\mathrm{rad},i,i+1} . \quad (18)$$

Using the one-dimensional heat conduction law and the linearized Stefan–Boltzmann law (5) we obtain:

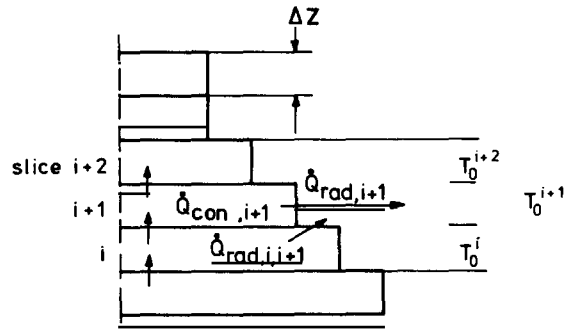

Fig. 3. The heat exchange in the slice model.

$$-\lambda_i \pi R_i^2 \left(\frac{\partial T_i(z)}{\partial z}\right)_{z=z_i} = -\lambda_{i+1} \pi R_{i+1}^2 \left(\frac{\partial T_{i+1}(z)}{\partial z}\right)_{z=z_i} + h_i (T_i - T_0^{(i)}) S_{i,i+1} ,$$

$$\text{for } i = 1, 2, ..., N-1 , \quad (19)$$

where $S_{i,i+1}$ is the area difference of the two slices. This factor enables us to evaluate any conical shape of the crystal especially the geometry of the transition from the seed to the neck and from the neck to the crystal.

If we insert the temperature distribution (14) into eq. (19) and eliminate A_i and B_i with eqs. (17a) and (17b), we finally obtain a set of $N-1$ equations in T_i. This equation system is nonlinear so as to include temperature dependency of the material constants and can only be solved numerically after performing the necessary rearrangement as described in ref. [22].

4. Radiation heat loss and the surrounding temperature

In the previous section it was shown that the energy balance is determined essentially by the energy loss due to the radiation *from* the crystal surface. On the other hand, the melt surface is radiating energy *to* the crystal surface. In this section, the balance of these two processes will be calculated, and the surrounding temperature $T_0(z)$, introduced previously, and important for the application of the Stefan–Boltzmann law, will be defined.

In a given direction which makes an angle ϕ with

the normal of an emitting surface, the flux of radiant energy is $I \cos\phi$ (J s^{-1} cm^{-2} sr^{-1}). If I is independent of the direction ϕ, the total radiation rate through half a sphere is:

$$W = \int_{\text{half sphere}} I \cos\phi \, d\omega = \pi I . \tag{20}$$

This is only valid in the case of rough surfaces (Lamberts law). For radiating metal surfaces this law does not hold exactly. Recent optical investigations of the radiation behaviour of growing copper crystals [11] show that the deviations from Lambert's law are small enough to be ignored.

This means that the radiation density rate is given by:

$$I = (\epsilon\sigma/\pi) T^4 . \tag{21}$$

In order to calculate the exchange of the radiation between two surfaces we choose the surface elements dA_1 and dA_2 according to fig. 4. Their normals form angles ϕ_1 and ϕ_2 with the connection line r. The energy rate radiated from surface dA_1 in the direction of dA_2 is given by:

$$d\dot{Q}_{1\to 2} = I_1 \, dA_1 \, dA_2 \frac{\cos\phi_1 \cos\phi_2}{r^2} . \tag{22}$$

Analogously for dA_2:

$$d\dot{Q}_{2\to 1} = I_2 \, dA_1 \, dA_2 \frac{\cos\phi_1 \cos\phi_2}{r^2} . \tag{23}$$

I_1 and I_2 are the radiation densities of the surface elements dA_1 and dA_2 respectively. In the following

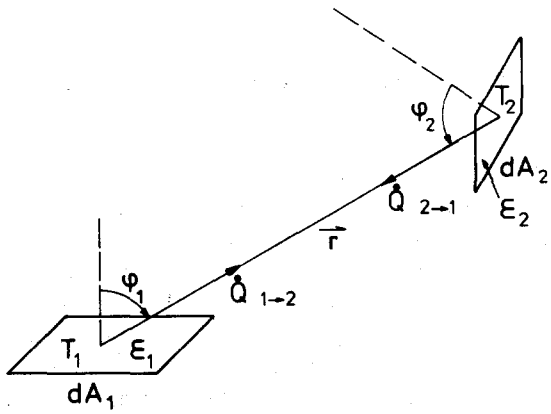

Fig. 4. The quantities for the determination of the heat exchange by radiation.

equation we omit reflection of the radiated energy. Then the energy loss per second of surface dA_1 in the direction of dA_2 is given by:

$$d\dot{Q}_1 = d\dot{Q}_{1\to 2} - \epsilon_1 \, d\dot{Q}_{2\to 1} ,$$

and after inserting eqs. (22) and (23):

$$d\dot{Q}_1 = (I_1 - \epsilon_1 I_2) \frac{\cos\phi_1 \cos\phi_2}{r^2} \, dA_1 \, dA_2 . \tag{24}$$

According to the temperature of dA_1 and dA_2, $d\dot{Q}_1$ is positive (heat loss) or negative (heat profit). For macroscopic surfaces this balance per unit area after insertion of expression (21) is:

$$\dot{q}_{\text{rad}} = \frac{\epsilon_1 \sigma}{\pi A_1} \int_{A_1} dA_1 \cdot \times \int_{A_2} dA_2 (T_1^4 - \epsilon_2 T_2^4) \frac{\cos\phi_1 \cos\phi_2}{r^2} . \tag{25}$$

(For an explanation of A_1, A_2, T_1 and T_2 see fig. 4; $\dot{q}_{\text{rad}}$ belongs to surface 1.)

If we apply this expression to the slices in the model (A_1 is the outer surface of a certain slice and T_R is its mean temperature), we obtain:

$$\dot{q}_{\text{rad}} = \epsilon_c \sigma T_R^4 \frac{1}{\pi} \int_{A_2} \frac{\cos\phi_1 \cos\phi_2}{r^2} \, dA_2 - \epsilon_c \sigma \frac{1}{\pi} \int_{A_2} \epsilon_2 T_2^4 \frac{\cos\phi_1 \cos\phi_2}{r^2} \, dA_2 . \tag{26}$$

The surface A_2 of the hemisphere can be divided into two parts:
(1) the furnace wall with temperature T_W (surface A_W),
(2) the melt surface with temperature T_L (surface A_L).

As the first integral in eq. (26) equals π, we can write:

$$\dot{q}_{\text{rad}} = \epsilon_c \sigma T_R^4 - \epsilon_c \sigma \epsilon_W T_W^4 \frac{1}{\pi} \int_{A_W} \frac{\cos\phi_1 \cos\phi_2}{r^2} \, dA_W - \epsilon_c \sigma \epsilon_L T_L^4 \frac{1}{\pi} \int_{A_L} \frac{\cos\phi_1 \cos\phi_2}{r^2} \, dA_L . \tag{27}$$

We are now able to define the view factors $f_{1,2}$ and $f_{1,3}$

for the melt:

$$f_{1,2} = \frac{1}{\pi} \int_{A_L} \frac{\cos\phi_1 \cos\phi_2}{r^2} \, dA_L \; ; \tag{28}$$

for the furnace wall:

$$f_{1,3} = \frac{1}{\pi} \int_{A_W} \frac{\cos\phi_1 \cos\phi_2}{r^2} \, dA_W \; . \tag{29}$$

Because of the $\cos\phi_1$ factor, the sum of the two integrals in (28) and (29) equals the area of the unit circle. Therefore the sum of the two view factors equals one (see ref. [12]):

$$f_{1,2} + f_{1,3} = 1 \; . \tag{30}$$

If we insert the expressions (28), (29), and (30) into expression (27), we obtain:

$$\dot{q}_{rad} = \epsilon_c \sigma \{ T_R^4 - [\epsilon_L T_L^4 f_{1,2} + \epsilon_W T_W^4 (1 - f_{1,2})] \} . \tag{31}$$

This equation corresponds to the Stefan–Boltzmann law, with the exception of the last term. On the other hand this last term has the dimension of a fourth power of the temperature, so the fourth root of the term can express the effective surrounding temperature T_0:

$$T_0 = [\epsilon_L T_L^4 f_{1,2} + \epsilon_W T_W^4 (1 - f_{1,2})]^{1/4} \; . \tag{32}$$

Nusselt [12] has developed a graphical method to calculate view factors. This method is applied to our problem as described in detail in ref. [22].

5. Convective heat loss: growth in a gas atmosphere

To calculate heat loss due to gas convection, we need to know the convection in the growth chamber. Although computation of the gas flow is very difficult, mathematical treatment of Czochralski growth under a gas atmosphere is possible by using an empirical relation concerning heat transport by convection. According to the authors of refs. [7] and [13], the equation for the heat loss of the crystal surface becomes:

$$\dot{q}_i = \epsilon_c \sigma (T_i^4 - T_0^{(i)4}) + \eta (T_i - T_{0,conv}^{(i)})^{1.25} \; . \tag{33}$$

The exponent 1.25 is valid for the case of natural convection [10]. If we linearize this equation, we obtain an additional term in expression (6), leading to:

$$h_i = \epsilon_c \sigma (T_i^2 + T_0^{(i)2})(T_i + T_0^{(i)}) + \eta \frac{(T_i - T_{0,conv}^{(i)})^{1.25}}{T_i - T_0^{(i)}} \; . \tag{34}$$

In principle, the gas temperature $T_{0,conv}^{(i)}$ can be measured with thermocouples, but this measurement is not very accurate, because the measured temperature is still influenced by radiation if we use an unshielded thermocouple. On the other hand, if we use shields to eliminate this radiation, the gas flow itself is influenced.

6. The numerical method for computation of the temperature field

As shown in section 3 we are able in principle to compute the temperature field in the crystal, but we also stated that the thermal surface resistance, one of the boundary values, is actually dependent on the temperature itself. In order to overcome this problem of the changing boundary conditions, the temperature field is calculated by an iteration method in the following way:

(A) The geometrical dimensions and the shape of the crystal are fixed.

(B) A set of arbitrary start values for the thermal surface resistances $\{R_{su}\}_j$ with $j = 1$ is guessed.

(C) With this set the temperature distribution $\{T(z)\}_j$ is computed.

(D) Using this distribution a new set of thermal surface resistances $\{R_{su}\}_{j+1}$ is computed.

(E) A next temperature distribution $\{T(z)\}_{j+1}$ is calculated.

(F) The average temperature distribution

$$\overline{\{T(z)\}_j + \{T(z)\}_{j+1}}$$

is calculated and compared with $\{T(z)\}_{j+1}$ at a certain location. If the difference at this location is less than 0.1°C the iteration process is stopped. Otherwise with this average temperature distribution a return to (D) is performed after incrementing j.

The convergence of this procedure is guaranteed, because an assumed thermal surface resistance, which is lower than the correct one, leads to a temperature

also lower than the correct one. This temperature gives then a thermal surface resistance which is higher than the correct one in the next iteration step and vice versa. A fast convergence is obtained by using the average temperature as the input for the next iteration step. In practice, the desired accuracy is obtained after the fourth cycle. Additional details of the method can be found in ref. [22].

From the resulting temperature field, the following quantities are calculated:
(1) the axial temperature gradient,
(2) the heat flow through the crystal,
(3) the heat flow at the surface of the crystal,
(4) the radial temperature gradient,
(5) the surface temperature,
(6) the thermal stresses,
(7) the bulk melt temperature,
(8) the interface curvature.

After the computation of these values, the program is started again with an increased crystal length. Therefore we get series of data as a function of the crystal length. Because the crystal length is proportional to the time, growth parameters can be expressed as a function of the time, too.

The accuracy of the calculated values is determined by:
(1) the slice thickness,
(2) the number of the significant digits of the computation.

For the determination of the optimum slice thickness, some computations have been carried out for a cylindrical crystal with different slice thicknesses and with 8 and 16 digits (single and double precision). Fig. 5 shows the results for the temperature gradient whereby it is clear that accurate values for thick slices cannot be obtained. If we decrease the thickness, the data tend toward a constant value for double precision programming. In the case of single precision the accuracy decreases for decreasing thickness because of the accumulation of the rounding errors. Therefore the computations were performed with double precision and with a slice thickness of 0.05 mm.

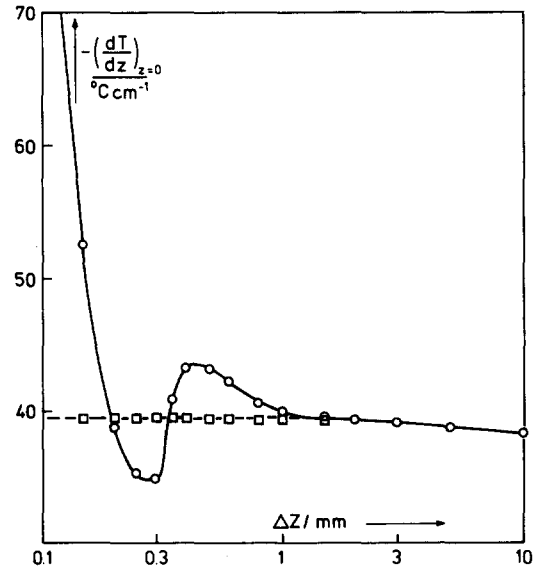

Fig. 5. The temperature gradient at the interface in the crystal as a function of the slice thickness: (○) single precision computation; (□) double precision computation.

7. The combination of the shape defining growth equations with the temperature distribution in the melt and in the crystal; derivation of some growth parameters

To calculate the growth parameters already mentioned we have first to investigate the temperature distribution in the melt and in the meniscus column which is attached to the growing crystal. In Czochralski growth the bulk material in the melt has to be heated up to a temperature above the melt temperature. This normally occurs by RF heating or resistance heating. In both cases the heat is generated round the outside of the melt and flows into the total volume of the bulk melt by heat conduction and convection. Experimental investigations for metals (and also for sodium chloride [14]) have shown that the temperature differences in the whole bulk are smaller than local temperature fluctuations caused by convection, which can be explained by assuming that the heat transport in the bulk melt is mainly controlled by convection. Therefore we can introduce a mean bulk melt temperature T_L valid for the whole bulk melt.

In the meniscus column the heat flow is controlled by a thermal boundary layer δ. Therefore the heat flow $\dot{Q}_1$ from the melt reaching the interface is given by:

$$\dot{Q}_1 = \pi R_1^2 \lambda_L (T_L - T_M)/\delta \,, \tag{35}$$

where R_1 is the crystal radius at the interface. We assume that this boundary equals the interface height h_{int} in the first approximation. This gives:

$$\dot{Q}_1 = \pi R_1^2 \lambda_L (T_L - T_M)/h_{int} . \quad (36)$$

This assumption is in contrast to that of Brice [5] who postulates a constant layer thickness δ. The correctness of our assumption has been proven earlier by the measurement of h_{int} as a function of $T_L - T_M$ and by the investigation of the step response of the interface position after a steplike change of the bulk melt temperature or the pulling speed [15]. This assumption, already postulated by Geist and Grosse [16] was also proved indirectly by Mühlbauer [17], who was thereby able to calculate the doping inhomogeneity caused by the measured sinusoidal temperature oscillations in the bulk melt. Finally it should be noted that this assumption is consistent with the experimental test for checking the theory [22].

Eq. (36) shows clearly that the interface height is controlled by the heat flow $\dot{Q}_1$ and the bulk melt temperature T_L.

The interface height determines the axial and radial growth in purely meniscus controlled growth, which means the shape of the growing crystal. Quantitatively this is expressed by the system of the shape defining differential equations:

$$\dot{z} = v_{eff} - \dot{h}_{int} , \quad (37a)$$

$$\dot{r} = (v_{eff} - \dot{h}_{int}) \operatorname{tg}[\alpha^*(h_{int}, R_1)] , \quad (37b)$$

where $v_{eff} - \dot{h}_{int}$ is the vertical microscopic growth rate and v_{eff} is the pulling speed corrected for the lowering of the melt level.

α^* is the angle between the vertical and the tangent at the crystal at the triple phase line and is related to the socalled joining angle α_j (angle between the vertical and the tangent at the meniscus) and the material dependent contact angle β (angle between the tangent at the crystal and the tangent at the meniscus) according to ref. [18]:

$$\alpha^* = \alpha_j - \beta .$$

For metals β is approximately zero [19].

The heat flow balance at the interface can be derived from the following reasoning. The heat flow by conduction in the liquid $\dot{Q}_1$ at the interface and the latent heat $\dot{Q}_3$ has to be conducted into the crystal by $\dot{Q}_2$ (see fig. 1):

$$\dot{Q}_1 + \dot{Q}_3 = \dot{Q}_2 . \quad (38)$$

After inserting the corresponding terms we obtain

$$-\pi R_1^2 \lambda_L \left(\frac{\partial T(z)}{\partial z}\right)_{L,z=0} + v\rho L \pi R_1^2 = -\pi R_1^2 \lambda_S \left(\frac{\partial T(z)}{\partial z}\right)_{S,z=0} . \quad (39)$$

Since the temperature gradient in the solid is known from the temperature field, the bulk melt temperature can now be evaluated:

$$T_L = T_M + h_{int}\left[-\frac{\lambda_S}{\lambda_L}\left(\frac{\partial T(z)}{\partial z}\right)_{S,z=0} - \frac{v\rho L}{\lambda_L}\right] . \quad (40)$$

Eq. (40) is the basic equation for the calculation of the bulk melt temperature–time program for a certain crystal shape.

The values of h_{int} as a function of the crystal radius and the joining angle calculated by Mika and Uelhoff [18], are used to compute the bulk melt temperature.

It is important to know something about the microscopic growth rate and the growth rate fluctuation with regard to the connection between the effective segregation coefficient and the growth rate [20]. However, the microscopic growth rate may alter for two reasons: through temperature fluctuations in the melt and during controlled changes of the interface height to shape the crystal. In our model we included only the controlled changes of the interface height in the computation of the microscopic growth rate.

Thermal stresses and strains can be calculated from the radial temperature gradient. In first approximation the radial dependence of the temperature is given by:

$$T_i(r) = T_i - \tfrac{1}{2} a_i r^2 , \quad \text{for } i = 1, 2, ..., N. \quad (41)$$

This expression satisfies the condition that $(\partial T/\partial r)_{r=0}$ equals zero. The constants a_i can be calculated by inserting this expression into the boundary condition (4b):

$$a_i = \frac{h_i}{\lambda_i R_i} (T_i - T_\delta^{(i)}) , \quad \text{for } i = 1, 2, ..., N. \quad (42)$$

This leads to the temperature difference between

axis and surface of slice i:

$$\Delta T_R^{(i)} = \frac{h_i R_i}{2\lambda_i} (T_i - T_0^{(i)}), \quad \text{for } i = 1, 2, ..., N. \quad (43)$$

The stress–strain relations and the equation for stress equilibrium in cylindrical coordinates can be obtained from ref. [21].

If the thermal stress is radially symmetric and the crystal is a cylinder with a radius R, then the boundary conditions are such that $\sigma_r = 0$ at $r = R$, and finite stresses are possible at $r = 0$.

Hence, with these boundary conditions, we are able to solve the stress equations:

$$\sigma_r = \frac{\alpha E}{1-\nu}\left(\frac{1}{R^2} - \frac{1}{r^2}\right) \int_0^R Tr \, dr, \quad (44a)$$

$$\sigma_\theta = \frac{\alpha E}{1-\nu}\left[\left(\frac{1}{R^2} - \frac{1}{r^2}\right) \int_0^R Tr \, dr - T\right], \quad (44b)$$

$$\sigma_z = \frac{\alpha E}{1-\nu}\left(\frac{2}{R^2} \int_0^R Tr \, dr - T\right). \quad (44c)$$

With the radial temperature distribution (41) we also obtain the strains for each slice:

$$\epsilon_r - \alpha T = \frac{1}{E}[\sigma_r - \nu(\sigma_\theta + \sigma_z)], \quad (45a)$$

$$\epsilon_\theta - \alpha T = \frac{1}{E}[\sigma_\theta - \nu(\sigma_r + \sigma_z)], \quad (45b)$$

$$\epsilon_z - \alpha T = \frac{1}{E}[\sigma_z - \nu(\sigma_r + \sigma_\theta)]. \quad (45c)$$

By calculating the temperature distribution close to the interface with the aid of the known axial and radial temperature gradients, the shape of the isotherm for the melting temperature is determined also by eq. (41). Because of the assumed rotational symmetry (non-faceting crystals) the isotherms are shell shaped. We can assume that the axial temperature gradient close to the interface is constant. Using eqs. (41) and (43) the temperature field $T_i(r, z)$ in this region is thus given by:

$$T_i(r, z) = \left(\frac{\partial T_i(z)}{\partial z}\right)_{z=0} z - \frac{\Delta T_R^{(i)}}{R_i^2} r^2 + T_M,$$

$$\text{for } i = 1. \quad (46)$$

If supercooling is omitted the temperature of the interface equals the melting temperature T_M. Therefore the equation of the interface shape is:

$$z(r) = \left(\frac{\partial T_i(z)}{\partial z}\right)_{z=0}^{-1} \frac{\Delta T_R^{(i)}}{R_i^2} r^2, \quad \text{for } i = 1. \quad (47)$$

From this equation we can achieve the radius of curvature of the interface:

$$R_{int} = \frac{1}{2}\left(\frac{\partial T_i(z)}{\partial z}\right)_{S, z=0} \frac{R_i^2}{\Delta T_R^{(i)}}, \quad \text{for } i = 1. \quad (48)$$

8. Computational results and discussion

The theory presented in the previous sections was used to compute the distribution of the temperature and some other derived growth parameters for copper crystals with the dimensions mostly grown in this laboratory. The diameters of these crystals were 1, 6 and 10 mm. We used only seed crystals with a diameter of 6 mm, clamped in a stainless steel seed holder.

The material constants we used are tabulated in ref. [22].

Fig. 6 shows the crystal shapes of 1, 6 and 10 mm crystals with the transition zones between crystal neck and seed and crystal boule, respectively, deter-

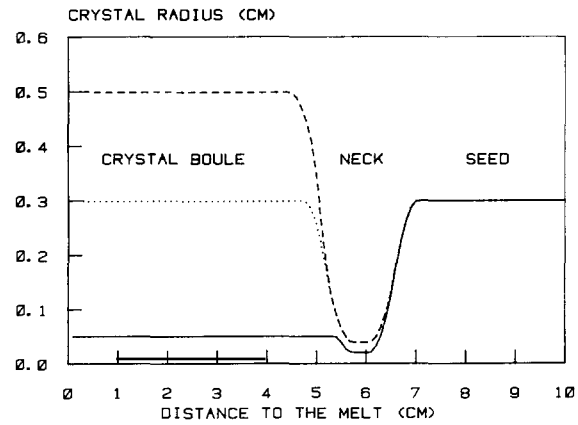

Fig. 6. Crystal shape as a function of the distance to the melt for a crystal length of 10 cm for a 1 mm diam. (dotted line), 6 mm diam. (dashed line) and 10 mm diam. (solid line) crystal.

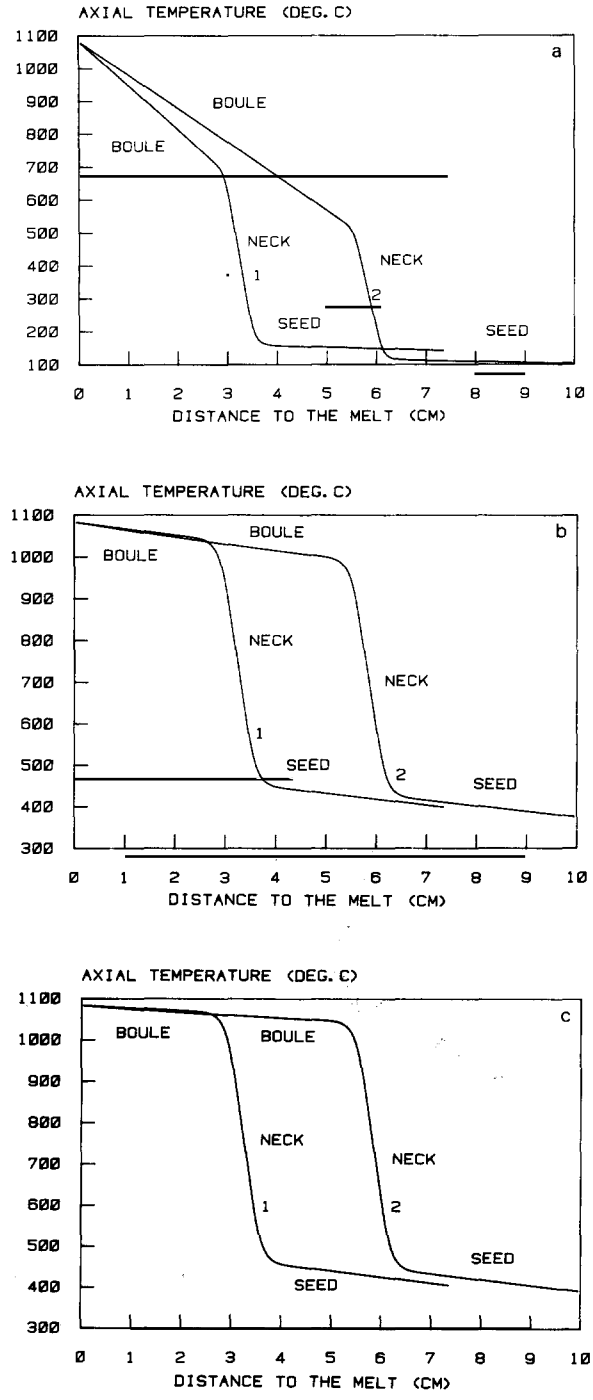

Fig. 7. The axial temperature distribution as a function of the distance to the melt for a crystal length of 7.4 cm (1) and 10 cm (2): (a) for a 1 mm diam. crystal; (b) for a 6 mm diam. crystal; (c) for a 10 mm diam. crystal.

mined by parabolic functions. The neck diameter for the 10 and 6 mm crystals was assumed to be 0.8 mm, a value slightly higher than the neck diameter of the 1 mm crystal (0.6 mm).

In figs. 7a–7c, the axial temperature distribution of the crystals is plotted for two different growth stages: in stage 1 the crystal boule has reached a length of 2.5 cm. In stage 2 this value is 5 cm. The figures show three important facts: the first two are visible from the slopes of the curves. Here, the temperature gradients in the boule and in the neck region of the 6 and 10 mm crystals are nearly independent of the crystal length. Only the 1 mm crystal shows a decrease of the temperature gradient in the neck and boule regions with increasing crystal length. This can be explained by the fact that in thin crystals most of the heat flowing into the crystal is radiated. Thirdly, though the seed holder is mounted on a watercooled pulling rod, the seed still shows a rather high temperature for the thicker crystals, due to the low thermal conductivity of stainless steel.

In figs. 8a–8c the maximum radial elastic strains are plotted. It is of some interest to note that the absolute values of the strains increase with increasing distances to the melt for thicker crystals. The strains reach their maximum at the beginning of the transition zone to the neck. The increase of the maximum strain value as a function of the distance to the melt is caused by the decreasing radiation energy obtained from the melt surface. In the 10 mm crystal, a strain of 2×10^{-6} is reached in this transition region, which should cause plastic microdeformation of the crystal. This result is quite different from the common assumption that the maximum stresses and strains always occur in the region immediately above the interface. From fig. 8c it should not be concluded that additional increasing of the crystal length would result in unlimited maximum strains: further computations have shown that for a certain value of the crystal length the absolute strain finally reaches a constant value. As expected the strains in the 1 mm crystals are smaller than in the thicker crystals. This result agrees with our observations that 1 mm crystals with low dislocation density even in the [110] direction could be grown.

With the model presented and the corresponding computer program we are able not only to analyze the above discussed local quantities for a certain crys-

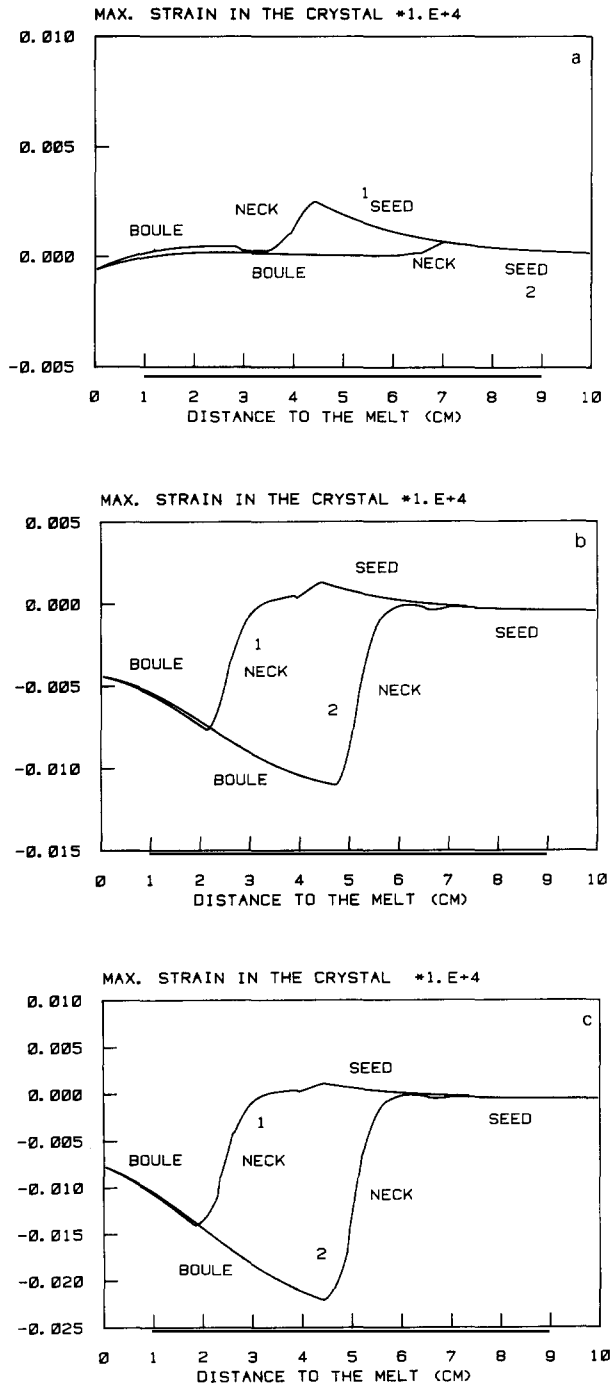

Fig. 8. Maximum radial strain in the crystal as a function of the distance to the melt for a crystal length of 7.4 cm (1) and 10 cm (2): (a) for a 1 mm diam. crystal; (b) for a 6 mm diam. crystal; (c) for a 10 mm diam. crystal.

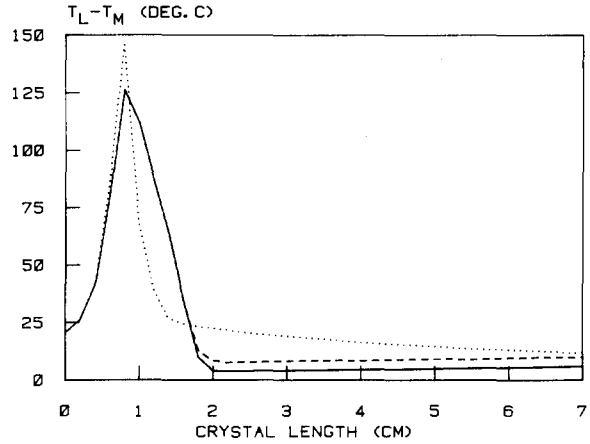

Fig. 9. The bulk melt temperature as a function of the crystal length for the three crystal diameters (the seed length of 3 cm is not included). Dotted line: 1 mm diam.; dashed line: 6 mm diam.; solid line: 10 mm diam.

tal length, but also to compute the actual values of these parameters at the solid–liquid interface as a function of the crystal length. These growth parameter of course can be related to the time, because of the simple relation between actual crystal length and time during the growth process.

In fig. 9 the computed bulk melt temperature (i.e. the difference between the melt temperature and the temperature of the melting point) is plotted as a function of the actual crystal length for the three discussed crystal shapes. One special result is clear: to obtain a crystal with constant diameter one has to increase the bulk melt temperature slowly for the thicker crystals but to decrease it for the 1 mm crystal when the necking process is finished (in our examples at a crystal length of 2 cm). The possibility to predict this function from the model is an important feature for automatic crystal growth, because by running such a temperature–time program, a desired crystal shape can be obtained.

In fig. 10 the heat flow into the crystal at the interface is shown. Again one can observe that after reaching the steady state growth at a length of 2 cm the heat flow increases for the thicker crystals, caused by an increase of energy radiation from the crystal boule. However, in the 1 mm crystal the heat flow decreases because the radiation loss of the boule is small compared to the heat flow through the

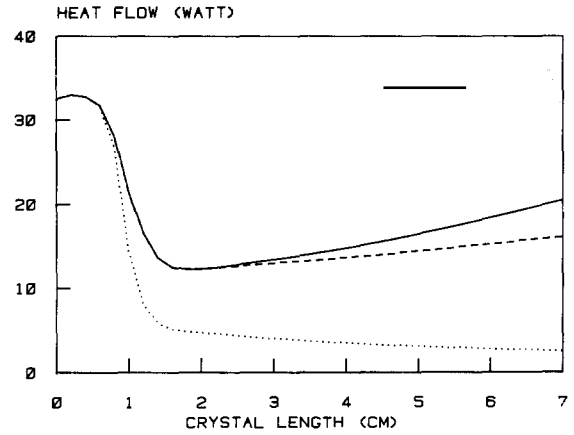

Fig. 10. The heat flow into the crystal at the interface as a function of the crystal length for the three crystal diameters. Dotted line: 1 mm diam.; dashed line: 6 mm diam.; solid line: 10 mm diam.

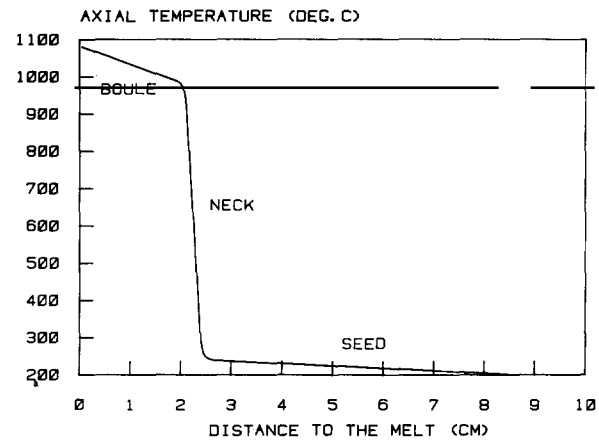

Fig. 12. Temperature distribution calculated with the slice model of the crystal shown in fig. 11.

crystal and the neck into the seed: because the thermal resistance of the crystal increases with increasing length, the heat flowing into 1 mm diameter crystal at the interface has to decrease.

We compared our growth model with that of Buckley-Golder and Humphreys [9] and studied the thermal conditions for a copper crystal with the same dimensions as taken by these authors. There was only one difference: in contrast to their model we had to take into account the existence of finite transition regions between seed, neck and crystal. Obviously this corresponds to a more realistic crystal. On the other hand this deviation in the crystal shape is one reason for the deviations between the results discussed below. (Any attemps to run our programs with a 90° change of the diameter in the neck region failed and ended with the computer message: "MELTED OFF"). The crystal shape as close as possible to that of ref. [9] is shown in fig. 11, where the distance between 3 and 9 cm is identical with the seed length. The axial temperature we obtained is plotted in fig. 12. This picture should be compared with fig. 2 in ref. [9] for the deviation between the two temperature distributions is remarkable. While the temperature of the seed of ref. [9] is higher than 900°C, with an average temperature gradient of the crystal of 9°C/cm our results were 250°C and 45°C/cm.

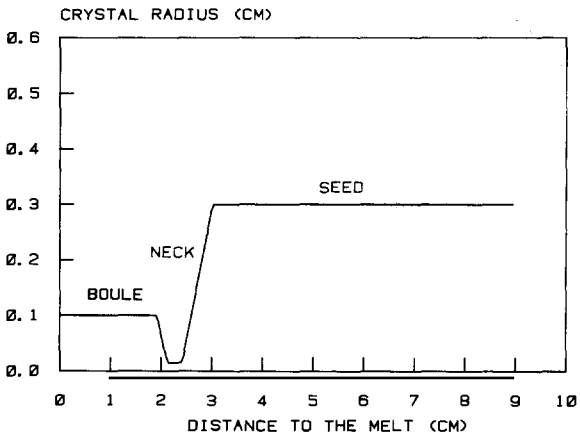

Fig. 11. Assumed crystal shape for the comparison with the theory of Buckley-Golder and Humphrey [9].

Such deviations in results indicate that there are some essential differences between the two models. The first one is that the authors [9] divide the total growing crystal into only three parts: seed, neck and crystal boule and in such a simplification the transition regions seed–neck and neck–crystal cannot be taken into account so that the temperature gradient at these two connections becomes infinite. The total heat flow balance becomes incorrect, at least to a certain degree. The second difference, an incorrect assumption in our opinion, is made by setting the seed temperature at the beginning of the seed equal

to the surrounding temperature. A further disadvantage of their model is due to an incorrect calculation of the heat dissipation by radiation: the heat radiation is proportional to $(T(z)^4 - T_0^4)$; T_0 is the surrounding temperature. However, for T_0, values have been used which were measured by thermocouples close to the crystal so that these tend to be values for the heat of the gas atmosphere. Nothing is said about the temperature of the pulling chamber which is the only receiver of the radiated heat. This means it is incorrect to say that the surrounding temperature for radiation exchange is equal to the gas temperature and equally incorrect that the crystal surface temperature is close to the surrounding temperature. Therefore it seems to us that some important assumptions in ref. [9] are invalid and that it is pretty impossible to develop heat flow theories for crystal growth based on constant Biot and Nusselt numbers as attempted by ref. [9].

In our model the most important omissions are (a) the finite values of $\partial T/\partial r$, (b) the curved geometry of the interface. However, it was proved afterwards that this practice was not erroneous when we tested the theory in the following manner: the calculated values of $\partial T/\partial r$ and the calculated shape of the interface were introduced into the Laplace equation which was then solved again. The differences between the original results and those so obtained were small enough to be ignored.

A new version of the model in preparation will contain improvements in two points: (a) by taking into account the exact meniscus shape to make the calculation of the heat exchange close to the interface in the melt even more accurate, and (b) in a reversal of the growth model. Until now, we have been able to predict geometrical and thermal parameters from a given crystal shape with our model, but sometimes it is desirable to determine the crystal shape which will be grown from a certain temperature–time program.

There was no opportunity to present any results about crystal growth of semiconductors or to discuss the influence of gas convection. This will be made up later on.

It should be stated briefly, that the following quantities can also be computed without difficulties: cooling rate, vacancy concentration, vacancy supersaturation and the distribution of the shear stresses in the different glide systems. Thus it seems to be possible to calculate important geometrical and thermal quantities together with some values related directly or indirectly to the generation of dislocations. However, one should be careful to draw direct conclusions only from the neck geometry and the temperature gradient in the neck when talking of the perfection of the crystal, as this was done in ref. [9]. Dyer showed in a recent paper [24] that behaviour of the dislocations in the neck region is much more complicated than assumed earlier [25]. Using these findings, Dyer was able for the first time to grow thick dislocationfree Si crystals with a [110] growth direction.

Our slice model can also be applied to the study of the floating-zone process. In this case the crucible radius has to be replaced by the maximum zone radius, and the interface height by the distances between the solid–liquid interfaces and the vertical location of the maximum zone radius. It would be interesting to compare the results of such a model with those obtained by Kuiken and Roksnoer [25]. Our resulting mathematics will have to be dealt with purely by numerical methods, but this does not seem to be a disadvantage. The thesis in ref. [25] that only analytical solutions are of general profit cannot be supported by the authors of this paper. The omissions and restrictions in analytical calculations are usually very wide-reaching. Quantitative results with sufficient accuracy can only be expected through the use of numerical calculations.

Acknowledgements

The computations were performed on the IBM 370-168 system of the "Zentralinstitut für Mathematik". The authors want to thank this institute for its excellent service. We are also grateful to Mrs. P. Gärtner for reading this paper critically and to Miss H. Mülheims for typing this paper.

Appendix

Glossary of symbols

i	Slice number
r, z	Cylindrical coordinates

t	Time
$T(r, z, t)$	Temperature dependent on r, z and t
$T(r, z)$	Temperature dependent on r and z
$T(z)$	Temperature dependent on z
$T_i(r)$	Radial distribution of the temperature slice i
$T_i(z)$	Temperature in slice i dependent on z
T_i	Temperature at the top of slice i at the axis of the crystal
$T_R^{(i)}$	Temperature on the outside of slice i
$\Delta T_R^{(i)}$	Temperature difference between the axis and the surface of the crystal
T_M	Melting temperature
T_L	Temperature of the melt
T_P	Temperature of the pulling rod
T_W	Temperature of the furnace wall
$T_0(z)$	Surrounding temperature dependent on z for radiation
$T_0^{(i)}$	Surrounding temperature of slice i for radiation
$T_{0,conv}^{(i)}$	Gas temperature close to slice i
z_c	z-Coordinate of the top of the crystal
z_i	z-Coordinate of the top of slice i
Δz	Thickness of one slice
l_{sh}	Length of the seed holder
R_{sh}	Radius of the seed holder
δ	Thermal boundary layer thickness
R_c	Crystal radius
R_i	Radius of slice i
R_{cr}	Crucible radius
R_b	Thermal resistivity
R_{su}	Thermal surface resistivity
h_{int}	Interface height above the melt surface
$\dot{Q}_{Index}$	In general heat flow
$\dot{q}_{Index}$	In general heat flow per unit area
$\dot{q}_{rad}$	Heat flow per unit area for radiation
$\dot{q}_{con}$	Heat flow unit per area for conduction
$\dot{q}_{conv}$	Heat flow per unit area for convection
$\dot{q}_{rad,i}$	Heat flow per unit area for radiation for slice i
$\dot{q}_{con,i}$	Heat flow per unit area for conduction for slice i
$\dot{q}_{conv,i}$	Heat flow per unit area for convection for slice i
$\dot{q}_i$	The sum of the radiation and convective heat loss per unit area of slice i
$\dot{Q}_{rad,i,i+1}$	Radiative heat loss due to the difference in the cross sections of slice i and $i+1$
$S_{i,i+1}$	The difference of the cross sections of slice i and $i+1$
N	Total number of the slices
A, B	Integration constants to be calculated by using the boundary conditions
A_i, B_i	Integration constants for slice i
v	Pulling speed
v_{eff}	Pulling speed corrected for the lowering of the melt level
L	Latent heat
$\lambda, \lambda_i, \lambda_S, \lambda_L$	Heat conductivity (i, slice number; S, in the solid; L, in the liquid)
ρ, ρ_i	Density (i, slice number)
c, c_i	Specific heat (i, slice number)
$\epsilon, \epsilon_W, \epsilon_L$	Emissivity (W, furnace wall; L, melt)
σ	Stefan–Boltzmann constant
$\sigma_r, \sigma_\theta, \sigma_z$	Stress components in cylindrical coordinates
$\epsilon_r, \epsilon_\theta, \epsilon_z$	Strain components in cylindrical coordinates
E	Young's modulus
ν	Poisson's ratio
α	Expansion coefficient
R_{int}	Radius of the interface plane
η	Coefficient of surface heat transfer

References

[1] A.W.A. van der Hart and B. Knook, in: Abstracts 1st European Conf. on Crystal Growth (ECCG1), Zürich, 1976.

[2] W. Uelhoff, A.W.A. van der Hart, A. Fattah, C. Hanke, K.J. Gärtner and J. Docter, in: Abstracts 2nd European Conf. on Crystal Growth (ECCG2), Lancaster, 1979.

[3] W. Uelhoff, Dissertation, Münster (1963).

[4] W.R. Wilcox and R.L. Duty, J. Heat Transfer, Trans. AIME 88C (1966) 45.

[5] J.C. Brice, J. Crystal Growth 2 (1968) 395.

[6] M. Lallemand, G. Lormand and M. Chevreton, J. Crystal Growth 43 (1978) 294.

[7] N. Kobayashi and T. Arizumi, J. Appl. Phys. 9 (1977) 361.

[8] N. Kobayashi, in: Preparation and Properties of Solid State Materials, Ed. R.A. Lefever (to be published).

[9] I.M. Buckley-Golder and C.J. Humphrey, Phil. Mag. A39 (1979) 41.

[10] H.S. Carslaw and J.C. Jaeger, Conduction of Heat in Solids (Clarendon, Oxford, 1959).

[11] A. van der Hart and W. Uelhoff, Optics, to be published.

[12] W. Nusselt, Z. Ver. Deutscher Ingr. 72 (1928) 673.

[13] E. Schmidt, Einführung in die technische Thermodynamik (Springer, Berlin, 1960).
[14] D. Fehmer, Diplomarbeit, Münster (1968).
[15] H. Wenzl and W. Uelhoff, Kristall Tech. 8 (1973) 1233.
[16] D. Geist and P. Grosse, Z. Angew. Physik 14 (1962) 105.
[17] A. Mühlbauer, Z. Naturforsch. 21a (1966) 490.
[18] K. Mika and W. Uelhoff, J. Crystal Growth 30 (1975) 9.
[19] H. Wenzl, A Fattah and W. Uelhoff, J. Crystal Growth 36 (1976) 319.
[20] J.C. Brice, The Growth of Crystals from the Liquid (North-Holland, Amsterdam, 1973).
[21] S. Timoshenko and J.N. Goodier, Theory of Elasticity (McGraw-Hill, New York, 1951).
[22] W. Uelhoff, A.W.A. van der Hart, A. Fattah, G. Hanke, D. Jedamzik, B. Knook, G.J. van der Berg and H. Wenzl, Report of the Kernforschungsanlage Jülich, Jül-1554, 1979.
[23] W. Uelhoff and K.J. Gärtner, in: (Cospar) Space Research, Vol. XIX, Ed. M.J. Rycroft (Pergamon, Oxford, 1979).
[24] D. Dyer, J. Crystal Growth 47 (1979) 533.
[25] H.K. Kuiken and P.J. Roksnoer, J. Crystal Growth 47 (1979) 29.